"giant faults" does not lead to total failure, because the displacement equivalent to the fault formation is complemented by elastic deformations around the fault as seen in Fig. 3F. Therefore, as plastic working proceeds, elastic strain energy is accumulated. The accumulation of the elastic strain energy is accompanied by the coordinated displacement of the zirconium and oxygen atoms as shown in Fig. 4. The nanometer-scale bending is discrete and accumulates into large crystal curvatures of a scale of several tens of micrometers, which indicate that the large elastic strain energy is accumulated discretely and hierarchically in the alloy. We conceive, for the time being, that all the dramatic changes in physical properties by cold working seen in Fig. 1 are attributed to this accumulated nanoscale discrete elastic strain energy.

References and Notes

1. J. C. Slater, *The Calculation of Molecular Orbitals* (Wiley, New York, 1979).
2. F. W. Averill, D. E. Ellis, *J. Chem. Phys.* **59**, 6412 (1973).
3. M. Morinaga, N. Yukawa, T. Maya, K. Sone, H. Adachi, in *Sixth World Conference on Titanium*, Societé Française de Metallurgie et des Materiaux, Cannes, France, 6 to 9 June 1988, P. Lacombe, R. Tricot, G. Beranger, Eds. (Les Editions de Physique, Les Ulis Cedex, France, 1989), pp. 1373–1379.
4. Materials and methods are available as supporting material on *Science* Online.
5. T. W. Duerig, A. R. Pelton, in *Materials Properties Handbook: Titanium Alloys*, R. Boyer, G. Welsch, E. W. Collings, Eds. (American Society for Metals International, Materials Park, OH, 1994), pp. 1035–1048.
6. C. Baker, *Metal Sci. J.* **5**, 92 (1971).
7. Y. Nakamura, *IEEE Trans. Magn.* **12**, 278 (1976).
8. E. P. Wohlfarth, *IEEE Trans. Magn.* **11**, 1638 (1975).
9. C. E. Guillaume, *Proc. Phys. Soc. London* **32**, 374 (1920).
10. R. Kainuma, J. J. Wang, T. Omori, Y. Sutou, K. Ishida, *Appl. Phys. Lett.* **80**, 4348 (2002).
11. R. F. Egerton, *Electron Energy-Loss Spectroscopy in the Electron Microscope* (Plenum, New York, 1986).
12. B. K. Teo, *EXAFS: Basic Principles and Data Analysis* (Springer-Verlag, Berlin, 1986).
13. H. Kitamura, *J. Synchrotron Radiat.* **5**, 184 (1998).
14. D. Vanderbilt, *Phys. Rev. B* **41**, 7892 (1990).
15. K. Laasonen, A. Pasquarello, R. Car, C. Lee, D. Vanderbilt, *Phys. Rev. B* **47**, 10142 (1993).
16. P. Hohenberg, W. Kohn, *Phys. Rev.* **136**, B864 (1964).
17. W. Kohn, L. J. Sham, *Phys. Rev.* **140**, A1133 (1965).
18. C. R. Krenn, D. Roundy, J. W. Morris Jr., M. L. Cohen, *Mater. Sci. Eng. A* **319–321**, 111 (2001).

Supporting Online Material

www.sciencemag.org/cgi/content/full/300/5618/464/DC1
Materials and Methods
Figs. S1 to S4
Table S1

30 December 2002; accepted 4 March 2003

Packing C_{60} in Boron Nitride Nanotubes

W. Mickelson, S. Aloni, Wei-Qiang Han, John Cumings, A. Zettl*

We have created insulated C_{60} nanowire by packing C_{60} molecules into the interior of insulating boron nitride nanotubes (BNNTs). For small-diameter BNNTs, the wire consists of a linear chain of C_{60} molecules. With increasing BNNT inner diameter, unusual C_{60} stacking configurations are obtained (including helical, hollow core, and incommensurate) that are unknown for bulk or thin-film forms of C_{60}. C_{60} in BNNTs thus presents a model system for studying the properties of dimensionally constrained "silo" crystal structures. For the linear-chain case, we have fused the C_{60} molecules to form a single-walled carbon nanotube inside the insulating BNNT.

Crystal structure is key in determining the mechanical, electronic, thermal, and magnetic properties of materials. Silicon, for example, is a modest bandgap semiconductor in its common diamond structure, but in its high-pressure simple hexagonal structure it is a metal and a superconductor (*1*). In low-dimensional nanostructures, crystal structure conspires with additional quantum mechanical confinement and surface effects to dictate the (often unusual) material properties. Of current interest is the ability to reliably manipulate atomic or molecular species into different nanoscale configurations, in which the crystal structure is dictated not only by interatomic or intermolecular interactions but also by self-imposed surface energy terms (such as in suspended metal nanowires) (*2*, *3*) or externally applied geometrical constraints [(with examples ranging from liquids freezing in confined geometries (*4*) to atoms assembled on surfaces (*5*)]. Because of its high symmetry and relatively weak intermolecular interactions, the fullerene C_{60} presents a near-ideal system for studying different crystal structures possible in a weakly interacting, dimensionally constrained system.

We here report unusual nanowire crystal structures of C_{60} obtained by packing the spherical fullerene molecules into the interior spaces of boron nitride nanotubes (BNNTs). BNNTs (*6–10*) have an energy gap of 5 eV independent of wall number, diameter, or chirality and thus constitute desirable insulating structures for geometrically and electronically confining atomic, molecular, or nanocrystalline species. We find that filling small-diameter BNNTs results in a linear chain of C_{60} molecules, analogous to previously observed carbon nanotube "peapods" (*11*), but with a significantly smaller C_{60}-C_{60} intermolecular distance. With increasing BNNT inner diameter, new stacking configurations are obtained that are unknown for bulk or thin-film forms of C_{60}. Our results are well accounted for by a simple geometrical model of hard spheres packed within a cylindrical cavity. Through postsynthesis treatment, it is possible to fuse the C_{60} molecules together into carbon nanotubes, yielding as a final product single-walled carbon nanotubes individually sheathed within electrically insulating BNNTs.

Pure BNNTs were first synthesized with either a plasma-arc discharge method (*9*), yielding primarily double-walled BNNTs, or a carbon-nanotube substitution reaction (*10*), yielding multiwalled BNNTs. The as-synthesized nanotube-rich soot was heat treated in air at 800°C for 20 min to remove excess boron nanoparticles and to open the tips of the BNNTs. The gray, heat-treated tubes were then sealed in an evacuated (10^{-6} torr) quartz ampoule together with commercially obtained C_{60} powder (MER Corp., Tucson, Arizona, 99.5%) in about a 5:1 C_{60}:BNNT mass ratio and uniformly heated to between 550° and 630°C for 24 to 48 hours. The ampoules were broken open, and the resultant black material was sonicated in either isopropanol or chloroform and deposited onto lacey-carbon grids for transmission electron microscope (TEM) characterization, with TOPCON 002B, Phillips CM200, and JEOL 2011 microscopes operating at electron energies typically near 100 keV.

Figure 1 shows TEM images of BNNTs treated with C_{60}. In Fig. 1A, two double-walled BNNTs are shown. The upper of the two tubes in Fig. 1A has an inner diameter of ~1.3 nm. The interior of this tube is well resolved and shows a linear chain of nearly evenly spaced C_{60} molecules. This hybrid structure is very similar in appearance to previously reported (*11*) single-walled carbon nanotube/C_{60} peapods. The lower BNNT in Fig. 1A is partially filled with amorphous boron nitride; this filling has substantially prevented C_{60} infiltration. Figure 1B shows additional TEM images of BNNTs treated with C_{60}. The lower half of the figure shows a five-walled BNNT with innermost diameter of 1.3 nm, which is efficiently filled with a linear chain of C_{60}.

Department of Physics, University of California at Berkeley, Berkeley, CA 94720, USA. Materials Sciences Division, Lawrence Berkeley National Laboratory, Berkeley, CA 94720, USA.

*To whom correspondence should be addressed. E-mail: azettl@socrates.berkeley.edu

The upper half of Fig. 1B shows a double-walled BNNT. The left and right portions of the tube interior contain amorphous boron nitride "plugs," whereas the central portion is completely empty. These plugs, present before filling, are confirmed to be boron nitride by electron energy-loss spectroscopy (EELS) and are impervious to C_{60} diffusion. The lack of C_{60} within the empty nanotube space thus suggests strongly that C_{60} molecules only enter BNNTs through the ends of the tube and not through the side walls.

The C_{60}-C_{60} intermolecular distance inside the BNNT, for both Fig. 1A and 1B, is 0.9 nm, which is slightly smaller than the 1.0-nm intermolecular distance for carbon peapods (*11*). This difference could be due to a large van der Waals attraction between the nanotube and the C_{60} or possibly to commensurability effects. However, there is a large discrepancy of the van der Waals energy between nanotubes and C_{60} ranging from –0.508 eV (*12*) to –3.26 eV (*13*) for a (10,10) carbon nanotube. Therefore, it is not possible to determine what effect is causing the decrease in the intermolecular distance.

We have also completely filled larger diameter BNNTs with C_{60}. The packing arrangement of the C_{60} is found to be very dependent on the tube diameter. Only for very large diameter tubes do the C_{60} molecules exhibit their bulk-crystal stacking geometry. The resulting C_{60} nanowires generally display structural characteristics unknown in bulk or film forms of C_{60}. Indeed, the resulting "crystal" structures are almost entirely dictated by the cylindrical confining geometry of the host BNNT.

Figure 2, A to D, shows TEM images of C_{60}-filled BNNTs with successively larger innermost tube diameter (ranging from 2.0 to 4.0 nm). In Fig. 2, A to C, the C_{60} nanowires appear to have a regular, one-dimensional crystal structure, whereas the wire of Fig. 2D has substantial disorder. The crystal structures of the C_{60} nanowires of Fig. 2, A to C, are all distinct, and indeed we have found many different C_{60} stacking configurations within BNNTs. The key parameter dictating the C_{60} stacking is the innermost BNNT diameter.

To elucidate how the C_{60} molecules stack as a function of innermost diameter, we have used a simple model in which hard spheres are packed in a minimum-energy (i.e., thermally annealed, maximum filling fraction) configuration inside a hard cylindrical cavity. Hard-sphere packing has been considered previously within parallel plates (*4*), on the inside of cylindrical surfaces (*14*), and in small-diameter cylinders (*15*). In our simplified model, the diameter of the spheres represents the diameter of C_{60} plus the average van der Waals distance. A first-order correction to the model would be to use two different van der Waals energy scales: one for C_{60}-C_{60} interactions, another for C_{60}-BNNT interactions. To gain rapid insight into the predictions of the simplified model, we packed glass spheres inside vertical quartz cylinders of various diameters. Even this simple model yields complex results (*15*), and we describe here only the most salient features. With the spheres individually just fitting inside the cylinder, the linear-chain or classic peapod configuration (e.g., Fig. 1) is reproduced. At slightly larger cylinder diameters, the spheres begin to form a staggered chain. At still larger diameters, the stagger becomes close packed, followed by a corkscrew-like structure. This structure persists until the diameter of the cylinder is exactly twice the sphere diameter, whereupon the spheres stack in radially oriented pairs successively rotated by 90° along the cylinder axis. At larger cylinder diameters, the spheres form another corkscrew-like structure, here called a 3-corkscrew. When the cylinder diameter is increased further such that a triangle of spheres just fits within the cylinder cross section, the spheres stack in a close-packed structure with the triangles successively rotated by 60° along the cylinder axis. With increasing cylinder diameter, this stacking pattern of planar n-polygons of spheres rotated by $360°/n$ between layers, followed by the $n + 1$ corkscrew-like structure at slightly larger cylinder diameter, continues until $n = 6$, beyond which disorder emerges. For small cylinder diameters, our findings are consistent with detailed computer simulations (*15*) performed for stacking hard spheres in a hard cylinder of diameter less than 2.155 sphere diameters.

For $n = 4$ and 5, the sphere crystal structures have a prominent empty channel down the center of the cylinder. For $n = 6$, the empty channel along the tube axis becomes just large enough to accommodate spheres; hence, for $n = 6$ there results an additional linear column

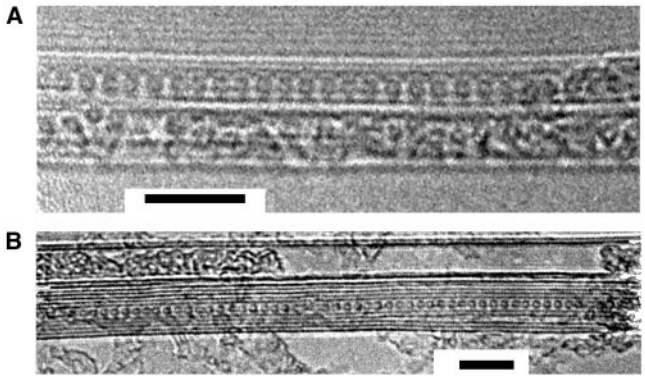

Fig. 1. High-resolution TEM (HRTEM) image of C_{60}-treated BNNTs. (**A**) A double-walled nanotube is filled with a linear chain of C_{60}. (**B**) A five-walled nanotube is similarly filled. The C_{60}-C_{60} center-to-center distance in both cases is ~0.9 nm. Bar, 4 nm.

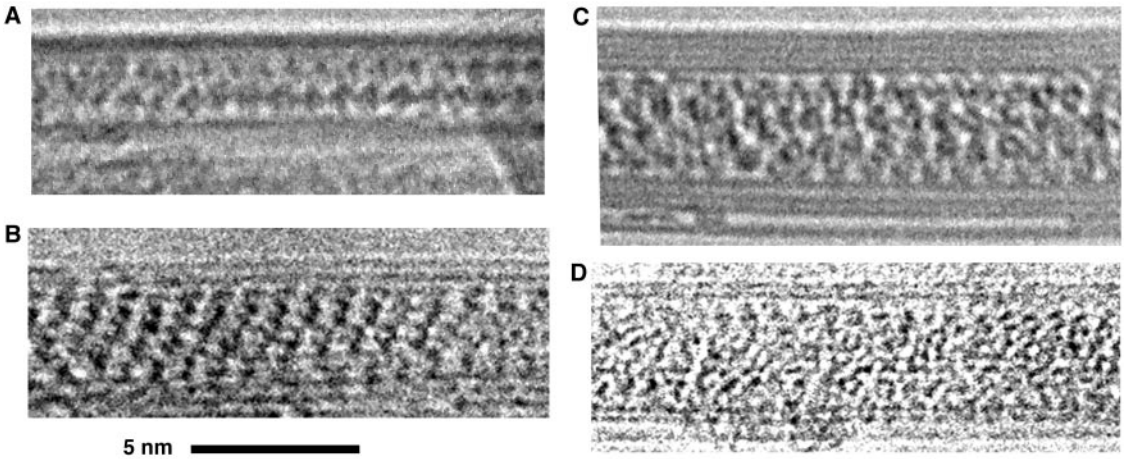

Fig. 2. HRTEM images of C_{60}-treated BNNTs. The nanotubes' innermost diameter, d, increases from (A) to (D), resulting in different C_{60} silo crystal structures. (**A**) $d = 2.0$ nm, with a staggered C_{60} nanowire; (**B**) $d = 2.8$ nm rotated triangles C_{60} nanowire; (**C**) $d = 3.3$ nm with a 7-corkscrew with two legs C_{60} nanowire; (**D**) $d = 4.0$ nm with disordered stacking of C_{60}. All magnifications are the same. Bar, 5 nm.

of spheres precisely down the center of the cylinder. The periodicity of this central column or linear chain is incommensurate with the axial periodicity of the outer spheres, and thus this structure, although still defect free, lacks any long-range translational order. Indeed, from a crystallographic point of view, such a "crystal" structure lies somewhere between a lattice-modulated structure containing two periodicities (e.g., a charge density wave) and a system lacking long-range translational order but having long-range orientational order (i.e., a quasicrystal). Because of the critical role here played by the geometrically confining walls in determining the final structure, we label these constructs "silo" crystal structures.

The emergence of disorder in the model just beyond $n = 6$ has a simple origin. At diameters larger than that which just accommodates the planar hexagon, the channel down the center of the cylinder has a diameter larger than a sphere diameter, which allows spheres filling the channel to shift off axis, forming a staggered column. The staggering in turn disturbs the ordering of the radially surrounding spheres, resulting invariably in disorder. Finally, when the cylinder diameter is very large, the boundary conditions imposed by the cylinder walls become insignificant and the spheres stack largely in a conventional crystalline close-packed manner.

The C_{60} nanowire stacking configurations of Fig. 2 exemplify these predictions. The BNNT of Fig. 2A has an inner diameter of 2.0 nm, not quite large enough to fit two C_{60} molecules side by side in a tube cross section. Therefore, the stacking order follows the staggered configuration described above. In Fig. 2B, the dominant BNNT (partially obscured by an independent overlapping nanotube) has an inner diameter of 2.8 nm, and here the C_{60} molecules stack in triangles, with each layer rotated by 60°. In Fig. 2C, the BNNT diameter of 3.3 nm allows C_{60} stacking in a 7-corkscrew configuration with two independent helices. There is a prominent stacking defect in the left region of this C_{60} nanowire, and the distortion wave from this defect propagates across many C_{60} molecules along the tube axis. Finally, the 4.0-nm BNNT of Fig. 2D displays only partial C_{60} order; the system is frustrated between low-*n* silo crystal order defined by the confining wall geometry and bulk C_{60} crystalline order defined by C_{60} intermolecular interactions.

Figure 3, A to C, shows idealized model representations for the silo crystal structures corresponding to Fig. 2, A to C, respectively (the defect of Fig. 2C has not been reproduced). Some of the silo crystal structures of Figs. 2 and 3 bear resemblance to those of suspended metal nanowires with helicity (*2*). However, the physics of these suspended metal nanowires is quite different in that, for the suspended wires, the absence of a "silo" or confining geometry and the exclusive dominance of interatomic and surface interactions dictate the structure.

Finally, we have investigated the stability of BNNT/C_{60} nanowire structures. In the case of carbon nanotube–based C_{60} peapod structures, it has been demonstrated (*16*) that electron beam irradiation can cause the C_{60} molecules to coalesce. We have explored analogous fusing of C_{60} within BNNTs using intense electron beam irradiation (Fig. 4). Starting with a single-chain nanowire structure (Fig. 4A), a 120-keV TEM electron beam was condensed (i.e., set to crossover) on the structure, yielding a current density of 400 nA/μm^2. After a few minutes the C_{60} molecules begin to dimerize (Fig. 4B). Then, after ~10 minutes, they have completely fused, forming an apparently crystalline, 0.62-nm-diameter tubular structure within the double-walled BNNT (Fig. 4C). BNNTs are stable under these irradiation conditions. EELS analysis confirms the carbon composition of the core. The TEM structural and compositional analysis allows us to identify the core tubular structure as a single-walled carbon nanotube. Unlike the case of fused carbon peapod structures in which a multi-walled carbon nanotube is invariably formed during the fusing, here the use of BNNT results in a carbon-nanotube core always sheathed by an insulating BNNT.

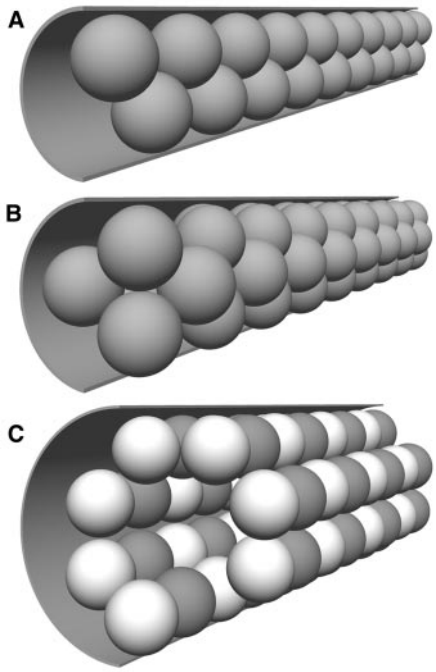

Fig. 3. Model predictions for hard-sphere packing within a hard cylinder. Images (**A** to **C**) correspond respectively to the C_{60} nanowire configurations of Fig. 2, A to C.

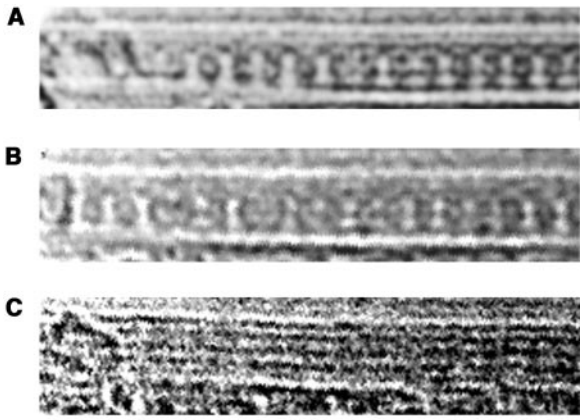

Fig. 4. Fusing of a linear chain of C_{60} into a single-walled carbon nanotube inside a BNNT. (**A**) A linear chain of C_{60} inside BNNT before fusing. (**B**) Dimerization of C_{60} after a few minutes of beam irradiation. (**C**) Complete fusion of C_{60} inside the BNNT, creating an insulated single-walled carbon nanotube.

References and Notes

1. K. J. Chang *et al.*, *Phys. Rev. Lett.* **54**, 2375 (1985).
2. Y. Kondo, K. Takayanagi, *Science* **289**, 606 (2000).
3. O. Gulseren, F. Ercolessi, E. Tosatti, *Phys. Rev. Lett.* **80**, 3775 (1998).
4. M. Schmidt, H. Lowen, *Phys. Rev. E* **55**, 7228 (1997).
5. T. Jamneala, V. Madhavan, M. F. Crommie, *Phys. Rev. Lett.* **87**, 256804 (2001).
6. A. Rubio, J. L. Corkill, M. L. Cohen, *Phys. Rev. B* **49**, 5081 (1994).
7. N. G. Chopra *et al.*, *Science* **266**, 966 (1995).
8. X. Blase, A. Rubio, S. G. Louie, M. L. Cohen, *Europhys. Lett.* **28**, 3085 (1994).
9. J. Cumings, A. Zettl, *Chem. Phys. Lett.* **316**, 211 (2000).
10. W. Q. Han, W. Mickelson, J. Cumings, A. Zettl, *Appl. Phys. Lett.* **81**, 1110 (2002).
11. B. W. Smith, M. Monthioux, D. E. Luzzi, *Nature* **396**, 323 (1998).
12. S. Okada, S. Saito, A. Oshiyama, *Phys. Rev. B* **64**, 201303 (2001).
13. L. A. Girifalco, M. Hodak, R. S. Lee, *Phys. Rev. B* **62**, 13104 (2000).
14. R. O. Erickson, *Science* **181**, 705 (1973).
15. G. T. Pickett, M. Gross, H. Okuyama, *Phys. Rev. Lett.* **85**, 3652 (2000).
16. D. E. Luzzi, B. W. Smith, *Carbon* **38**, 1751 (2000).
17. This research was supported in part by the National Science Foundation and by the Director, Office of Energy Research, Office of Basic Energy Sciences, Materials Sciences Division of the U.S. Department of Energy, under contract DE-AC03-76SF00098, administered by the sp^2 and Interfacing Nanostructures Initiatives. We thank T. S. Jespersen and N. Bodzin.

14 January 2003; accepted 4 March 2003